J. Fluid Mech. (1985), *vol.* 158, *pp.* 489–509
Printed in Great Britain

The turbulent mixing layer: geometry of large vortices

By F. K. BROWAND AND T. R. TROUTT†
Department of Aerospace Engineering, University of Southern California, Los Angeles, CA 90089-0192

(Received 4 January 1984 and in revised form 12 February 1985)

Several means for visualizing large-scale vortex structure in a turbulent mixing layer are proposed. Most of the observations are recorded along the low-speed side of the mixing layer, external to the rotational portion of the flow. Conventional correlation measurements in both the streamwise and spanwise directions indicate that the vortex structure becomes independent of the downstream coordinate in a non-dimensional distance of order $\lambda x/\theta_i = 300$–400, where $\lambda = \Delta U/2\overline{U}$ is the speed ratio and θ_i is the initial integral thickness. Simultaneous hot-wire measurements at 12 spanwise positions allow computer reconstruction of the velocity field as a function of span and time. These visualizations show the vortex structures to be primarily aligned across the span of the flow, but to contain irregularities. Spanwise correlation lengths are of the order of 3–$5\delta_\omega$ (δ_ω is the local vorticity thickness). However, the large vortices typically have lengths of order $20\delta_\omega$ when the irregularities along the span are ignored.

1. Introduction

Attention is focused on the large spanwise vortices in a mixing layer that were first described by Brown & Roshko (1971, 1974) and Winant & Browand (1974), and which have since been observed and studied in numerous investigations. It is plausible to assume that these vortices – so prominent in visualizations – must also be important dynamically. There is much accumulating evidence to demonstrate that the vortices are most energetic themselves, and, during interactions, control the energy transfer from the two streams to the turbulence (these points have recently been discussed by Browand & Ho 1983). The dramatic response of the mixing layer to the application of a small spatially coherent perturbation can only be understood with recourse to the presence and enhancement of spanwise vortex structure (cf. Hussain & Zaman 1981; Wygnanski & Oster 1982; Ho & Huang 1982).

The present study attempts to define the geometry of the large vortices. The flow is allowed to develop from a laminar boundary layer, or from an intentionally tripped turbulent boundary layer, but no other forcing is provided. In both cases the downstream structure becomes indistinguishable. The Reynolds numbers of the flow are large: $\Delta U\delta_\omega/\nu$ varies from about 3000 at the origin of the mixing layer to 1.5–2.0×10^5 at a distance of one metre downstream. The latter value corresponds to length Reynolds numbers $\Delta U x/\nu$ of 1.2–1.5×10^6. The spanwise extent of the flow is also made large intentionally – so that spanwise features will not be influenced by

† Permanent address: Department of Mechanical Engineering, Washington State University, Pullman, WA 99164-2920.

walls. Measured in units of local vorticity thickness $\delta_\omega = \Delta U/(\mathrm{d}\overline{u}/\mathrm{d}y)_{\max}$, the span is never less than $7\delta_\omega$ at the farthest downstream station.

The hot-wire arrays, placed on the low-speed edge of the flow, do not resolve features that have a spanwise scale smaller than the local mixing-layer thickness. Again, our interest is the three-dimensionality of the spanwise vortices, which are generally many mixing-layer thicknesses in length. Of course three-dimensionality extends to much smaller scales. There have been a number of recent papers that explore this smaller structure in detail: for example, Konrad (1976), Breidenthal (1981), Bernal *et al.* (1979), Bernal (1981) and Jimenez, Martinez-Val & Rebollo (1979). Wood & Bradshaw (1982) propose a typical vortex structure which bears considerable resemblance to the streamwise vortices observed and discussed earlier by Bernal. The presence of these features is not inconsistent with our present observations – they simply represent smaller-scale topography.

2. Experimental apparatus; techniques

2.1. *Wind tunnel*

A sketch of the wind tunnel is shown in figure 1. Flow properties have been carefully described in Browand & Latigo (1979). A series of cloth meshes (polyester silk-screen material) were added to the low-speed (upper) half of the stilling-section inlet to provide additional resistance, resulting in speed ratios $\lambda = \Delta U/2\overline{U} = 0.41, 0.56, 0.65$ and 0.81. The flow was uniform across the span to within 0.25 % of the maximum velocity in either stream, and the turbulence level $u'/\Delta U$ in the plane of the plate trailing edge was 0.3 % in the low-speed stream and less than 0.1 % in the high-speed stream. The high-speed-stream velocity was typically 25 m/s, and the equivalent flat-plate Reynolds number at the splitter-plate trailing edge was about 10^6 with no bursting observed. In most cases the mixing layer was allowed to develop from the initial laminar flow. For one speed ratio, $\lambda = 0.65$, the plate boundary layer was tripped using a cylindrical wire of diameter 1.6 mm placed 15 cm upstream of the trailing edge – resulting in a fully turbulent boundary layer at the origin of the mixing layer.

2.2. *Detection of structure*

Many of the results to be described utilize the longitudinal velocity fluctuations measured by a rake of hot wires placed on the low-speed side of the mixing layer near $y/\theta = 6$, where θ is the local integral mixing-layer thickness (see (1) in §3.1). In some cases the wires are placed along the ray $y/\theta = 6$ extending from the origin; in other cases the wires are placed along the span of the flow, at fixed x. Alignment of the spanwise array was accomplished by first setting the wires along a line parallel to the plate trailing edge with a relative accuracy ± 0.1 mm using a telescope. The entire array, supported on an old lathe bed, was then positioned downstream using our measurements of local mixing-layer thickness as a guide.

The ray $y/\theta = 6$ was chosen as the most appropriate position to detect structure within the mixing layer. Here the signals are sensitive to the longitudinal fluctuation associated with the large vortices passing underneath, but are not contaminated by the small-scale features within the rotational portion of the flow. In practice there is a relatively narrow range of y/θ where this technique may be successfully applied. Closer than $y/\theta = 6$ the intermittent rotational bursts are unacceptable. (According to Wygnanski & Fiedler (1970), the intermittency at $y/\theta > 5$ is less than 0.5 %.) Beyond $y/\theta \approx 8$ the signals are too small in amplitude to be useful.

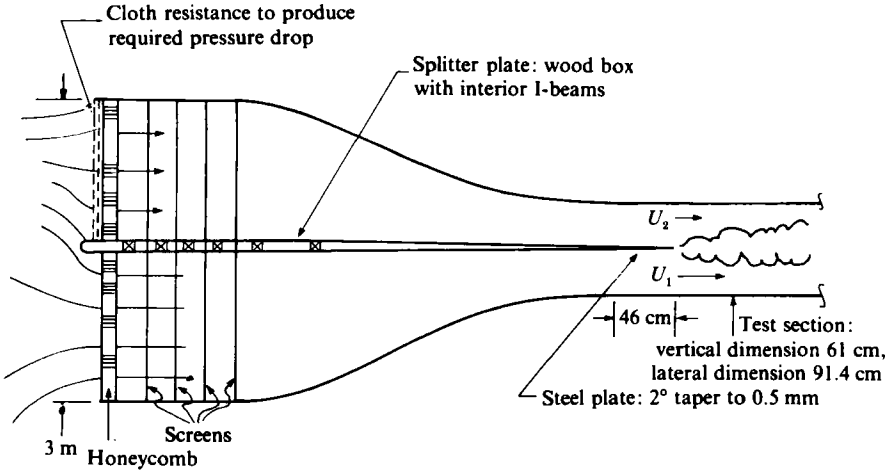

FIGURE 1. Schematic of wind tunnel.

The longitudinal fluctuation at the edge of the mixing layer is a summation of contributions from all the vortices comprising the mixing layer. However, the contribution from the vortex passing immediately underneath (nearest vortex) is much larger than the contributions from neighbouring vortices. A rough estimate can be obtained by considering the mixing layer as a row of two-dimensional line vortices (non-pairing vortices of appropriate circulation) spaced $4.3\delta_\omega$ apart. The ratio of the contribution from the vortex immediately below to the contribution of the next-nearest neighbour is then

$$\left[\left(\frac{y}{4.3\delta_\omega}\right)^2+1\right]\Big/\left(\frac{y}{4.3\delta_\omega}\right)^2.$$

For $y = 6\theta = 1.3\delta_\omega$, this ratio is larger than 10.

Further experimental verification that the fluctuation is a sensitive local measurement can be obtained from the signals themselves. Figure 2 shows traces taken simultaneously at eight downstream positions along the ray $y/\theta = 6$. The signals are well above noise level, with turbulent intensities $u'/\Delta U = 0.01$–0.02. Each signal exhibits a characteristic frequency – the local frequency of vortex passage. The timescale for each downstream position has been increased in proportion to the local mixing-layer thickness. With this scaling, the significant frequencies are in rough correspondence all along the mixing layer. The signal at the farthest-downstream station differs in timescale by a factor of almost 30, yet looks cleaner and resembles the initial instability more than do some of the intervening traces. Finally, figure 3 gives autocorrelation functions computed from data at $x/\theta_i = 1355$ for three values of y/θ. The average passage period T_p is associated with the time interval to the first peak. It can be seen that the time interval is not sensitive to the particular value of y/θ near $y/\theta = 6$. At $y/\theta = 4$ small-scale fluctuations reduce the degree of correlation, but even here there is little effect upon the computed average passage period.

2.3. *Digitization*

The hot-wire response was flat to at least 10 kHz. The hot-wire signals were first recorded on FM tape. Later these signals were digitized (12 bit conversion) and rewritten to digital tape. In some cases the FM tapes were played at a slower rate

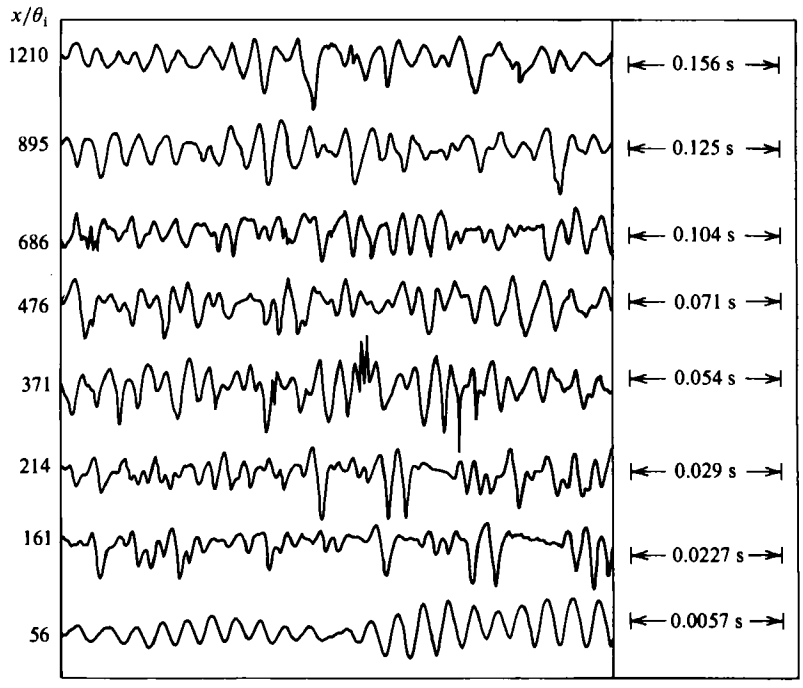

FIGURE 2. Longitudinal velocity fluctuations at various downstream positions along the ray $y/\theta = 6$.

to expand the timescale. Various combinations of tape speed and digitization rate resulted in real-time rates of 2000–10000 digitizations per second per channel. The signals were digitized unfiltered, since very little high-frequency content was present. The fluctuating voltage was defined for each hot wire by subtracting the computed mean value, and normalizing by the computed r.m.s. value. No calibration relating hot-wire fluctuation voltage to fluctuation velocity was needed, because these two quantities are linearly related for small fluctuation amplitude.

3. Results

3.1. *Mean growth of the mixing layer*

The mean thickness of the mixing layer is best determined by calculating the integral scale

$$\theta(\Delta U)^2 = \int_{-\infty}^{\infty} [U_1 - \overline{u}(y)][\overline{u}(y) - U_2]\,\mathrm{d}y. \tag{1}$$

Our results for various speed ratios are shown in figures 4(*a–c*). Figure 4(*a*) contains the raw data – integral thickness versus downstream distance. Close to the origin, the spreading rate $\mathrm{d}\theta/\mathrm{d}x$ is about the same for all speed ratios. Farther downstream, the growth rates approach a linear dependence upon x, and separate such that slower growth rates correspond to lower values of speed ratio λ. The linear dependence upon x is a requirement when no other lengthscales are relevant, but the dependence upon λ cannot be obtained from dimensional arguments. It may be understood by referring to the case of timewise growth. Imagine a mixing-layer sheet that is infinite in extent and becoming thicker with time. Neglecting viscosity, the thickness of the sheet must

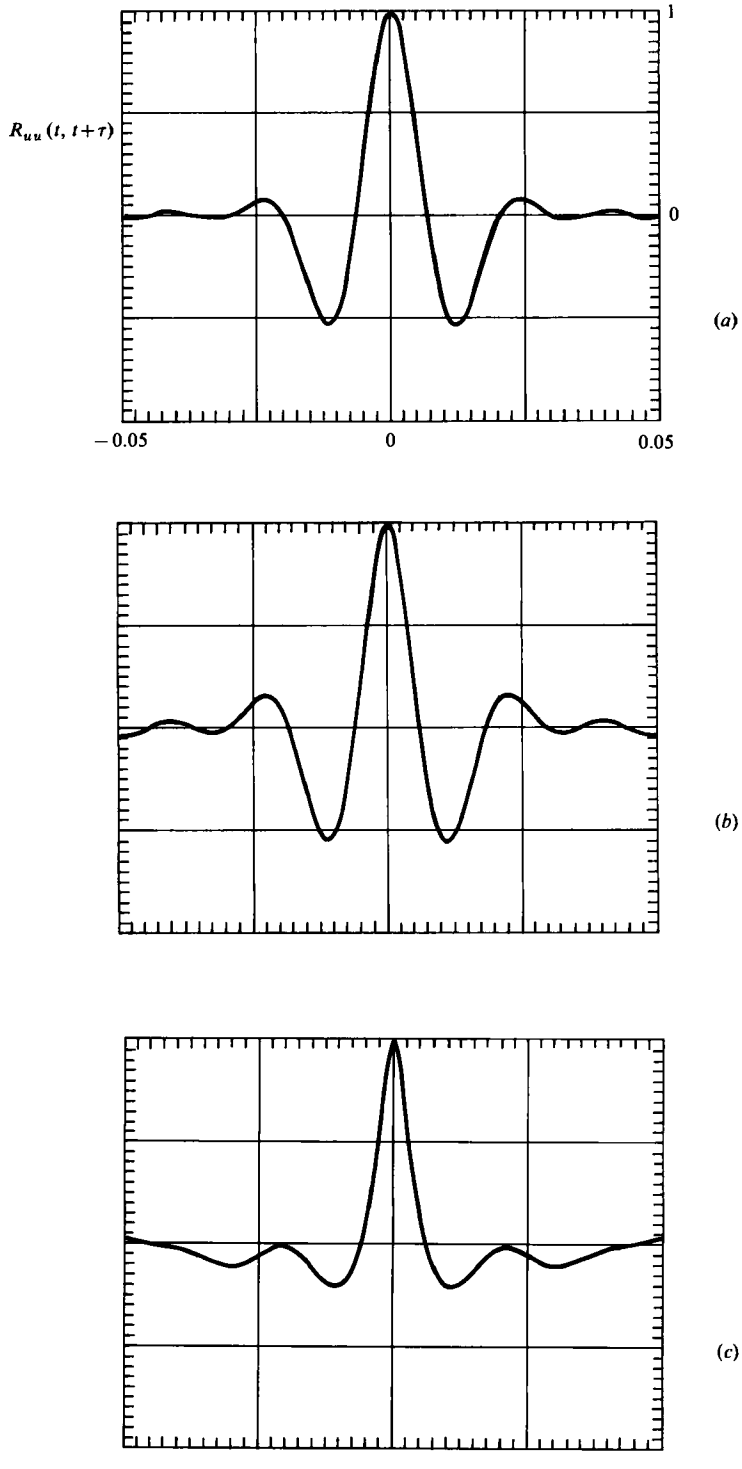

FIGURE 3. Autocorrelation of the longitudinal-velocity fluctuation at $x/\theta_i = 1355$ for three vertical positions: (*a*) $y/\theta = 8$; (*b*) 6; (*c*) 4.

be linearly proportional to the velocity difference and the time, since these are the only parameters available:

$$\theta(t) \sim \Delta U t. \tag{2}$$

A pseudo-spacewise growth is obtained by replacing t by $x/\overline{U}$. This Galilean transformation cannot be applied rigorously to the mixing layer growing from an origin in space, but the argument does predict the correct linear dependence upon x and suggests a linear dependence upon speed ratio:

$$\theta(x) \sim \frac{\Delta U x}{\overline{U}} \sim \lambda x. \tag{3}$$

When downstream distance is scaled by the speed ratio, the results appear as in figure 4(*b*). Far from the origin, the data are reasonably well correlated by this scaling, and appear to follow the linear law. Close to the origin, there is a pronounced hump – first a more rapid growth, then slower growth before approaching the downstream growth rate from below. The lower the speed ratio, the more pronounced the hump appearance.

The previous results imply that, in the initial region, another lengthscale must be important. We choose for this length an equivalent initial integral thickness θ_i. The adjective equivalent is used because θ_i is not measured directly. There is ambiguity in a direct measurement since the velocity profile near the origin is wake-like owing to the presence of boundary layers on the upper and lower surfaces of the splitter plate. Our initial θ_i is an effective integral thickness determined by measuring the frequency of the initial instability. This initial instability is assumed to produce an initial vortex structure having a passage frequency (or wavelength) appropriate to the most-amplified wave predicted from the spatial-stability calculations of Monkewitz & Huerre (1982). The prediction can be used to infer the thickness of the basic laminar shear flow. An alternative interpretation is that the inverse of the initial frequency is a direct measure of the lengthscale of the initial vortex structure, which is the most important scale in the problem. The values of θ_i determined in this manner are, in most cases, very close to the measured values of the boundary-layer momentum thickness on the high-speed side at the plate trailing edge. We have therefore taken the initial thickness to be the mean of these two measures, with a probable error of only a few per cent.

Figure 4(*c*) shows integral thickness and downstream distance scaled with initial integral thickness. The uncertainty associated with the errors in θ_i could move the data points along the diagonal lines shown in the plot. The results are consolidated over those of figure 4(*b*) by this non-dimensionalization. There appears to be a dependence upon λ near the origin which gradually disappears. All of the results relax to a single universal linear growth-rate curve beyond

$$\frac{\lambda x}{\theta_i} \approx 400\text{–}500.$$

Collectively the results are still well fitted by a line of slope

$$\frac{\mathrm{d}\theta}{\mathrm{d}x} = 0.034\lambda \tag{4}$$

in the region $\lambda x/\theta_i > 500$, which is the value quoted earlier by Browand & Latigo (1979) for $\lambda = 0.695$. It is equivalent to a growth rate for the vorticity thickness of

$$\frac{\mathrm{d}\delta_\omega}{\mathrm{d}x} = 0.17\lambda. \tag{5}$$

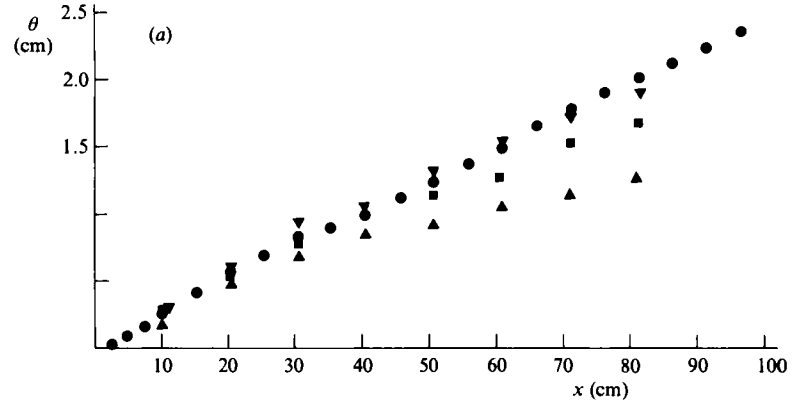

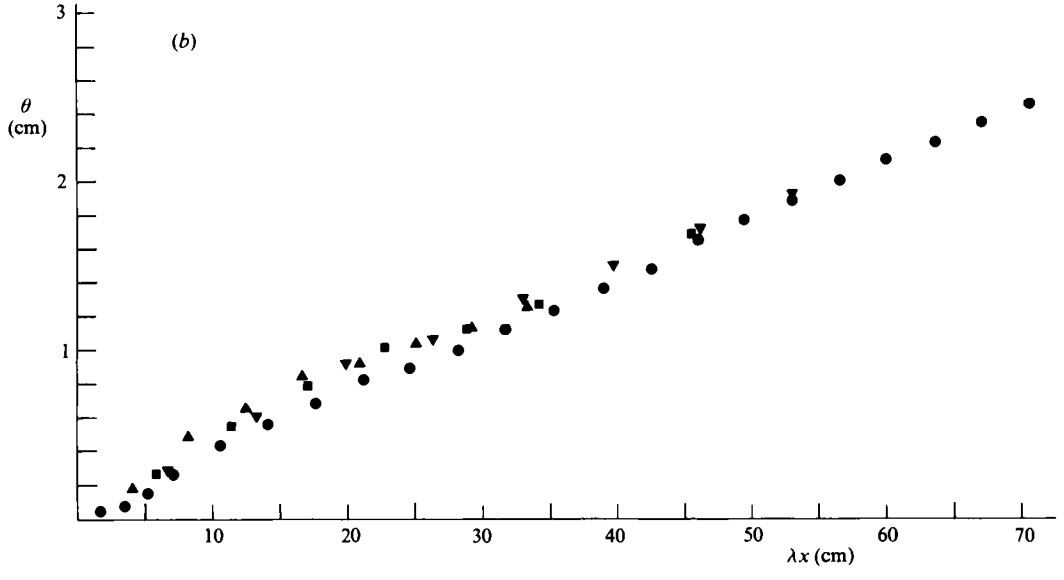

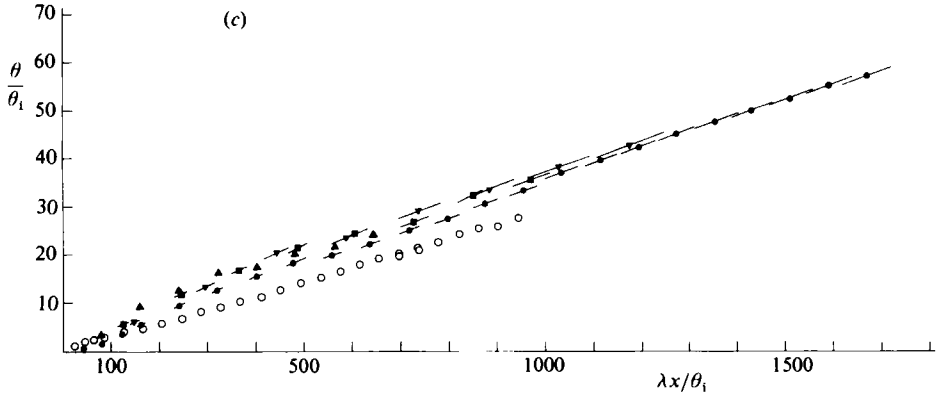

FIGURE 4. Mean downstream growth of mixing layer for various speed ratios: ●, $\lambda = 0.695$; ○, 0.695 (turbulent boundary layer); ▼, 0.65; ■, 0.56; ▲, 0.41. (*a*) Raw data. (*b*) Downstream distance scaled with speed ratio. (*c*) Non-dimensional presentation.

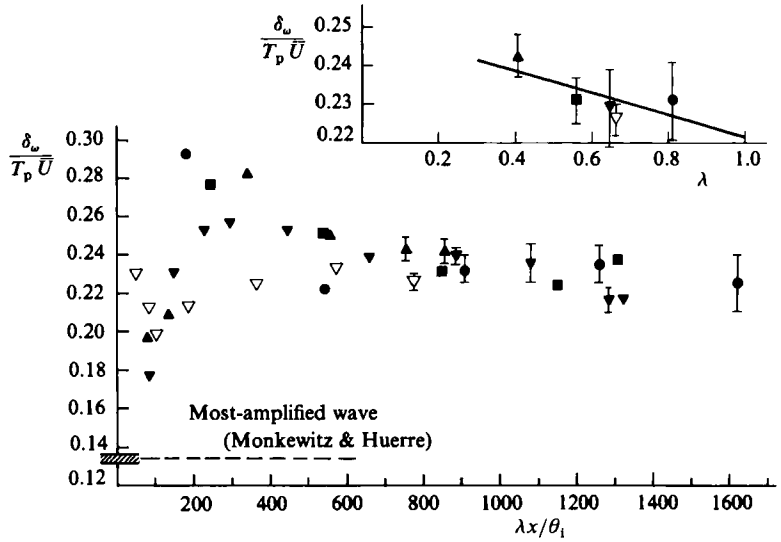

FIGURE 5. Strouhal number versus normalized downstream distance. Data recorded on the low-speed side at $y/\theta = 6$. Bars indicate estimated variance obtained from data at different spanwise locations. Open symbols denote tripped boundary layer. Most-amplified linear-wave estimate from Monkewitz & Huerre (1982).

The differences in growth rate near the origin – as much as 60 % – could easily account for the scatter in growth rates observed by various experimenters (cf. Brown & Roshko 1974). The physical reason for the more rapid initial growth is probably related to a localization of the pairing process. When the initial mixing layer is laminar, the first pairing (or several pairings) may take place with slightly more organization, and therefore less spatial jitter, than those pairings that occur farther downstream. If the mixing layer were made turbulent initially by tripping the boundary layer on the plate, one might expect a disappearance of the rapid-growth region near the origin. This is borne out by the results for a tripped boundary layer at $\lambda = 0.695$ (plotted as open symbols in figure 4*c*). In fact, the growth rate is initially much lower for the turbulent boundary layer, and it is concluded that the initial turbulence must interfere with pairing in the region near the plate (Browand & Latigo 1979). The slopes farther downstream are close (but not identical); the dominance of the vortex structure is eventually established. The total thickness of the mixing layer depends upon different growth histories, however, and remains smaller for the turbulent initial condition.

3.2. *Mean vortex spacing*

Another indication that a transition to asymptotic structure occurs near $\lambda x/\theta_i \approx 400$–$500$ is obtained from autocorrelations of velocity fluctuations along the ray $y/\theta = 6$. Again the mean vortex-passage period T_p is defined as the time interval to the first peak of the autocorrelation function. These passage periods are non-dimensionalized with the measured vorticity thicknesses δ_ω and the mean speed $\overline{U}$ to form Strouhal numbers $St = \delta_\omega / T_p \overline{U}$, plotted in figure 5 for various values of speed ratio. The results show the considerable variation of Strouhal numbers with downstream distance in the region near the origin, and the much smaller variation farther downstream. For reference, the most-amplified wave has a Strouhal number close to 0.135, according to linear-stability theory (Monkewitz & Huerre 1982). The Strouhal numbers in the experiment begin near the linear-stability value, increase

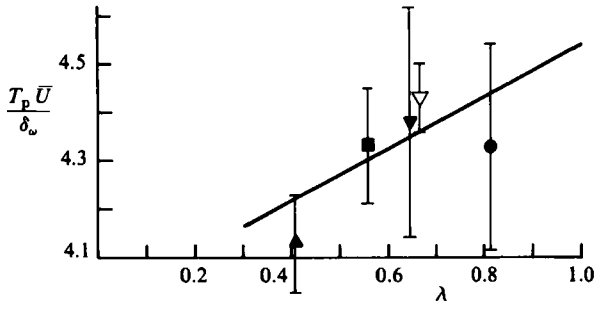

FIGURE 6. Average separation of vortices as a function of speed ratio. Data recorded on the low-speed side at $y/\theta = 6$.

to a peak in the vicinity of $\lambda x/\theta_1 \approx 200$–$300$, and finally relax slowly to intermediate values. The relaxation takes place at a non-dimensional distance of $\lambda x/\theta_1 \approx 400$–$500$. The exception is the flow with turbulent initial boundary layer. There is first a decrease in the local Strouhal number, then a gradual relaxation to a slightly larger value.

An asymptotic Strouhal number, determined by averaging values for downstream distances $\lambda x/\theta_1 > 600$, is plotted as a function of speed ratio (insert in figure 5). There seems to be a slight decrease in Strouhal number with increasing speed ratio. If $\delta_\omega/T_p \overline{U}$ were measured at the same y/θ on the high-speed side (far downstream), the value would be approximately 0.30. This difference can be understood simply. When the probe is on the low-speed side, vortices that are nearer and therefore travelling more slowly are given greatest weight. With the probe on the high-speed side, the opposite is true. The average of these two values, $\delta_\omega/T_p \overline{U} \approx 0.26$–$0.27$, would be a better measure of the average Strouhal number at a speed ratio of 0.65.

The quantity $T_p \overline{U}$ can be thought of as the spacing between vortices. Figure 6 shows this spacing, expressed in units of mixing-layer thickness, as a function of speed ratio. The spacing appears to increase with increasing speed ratio, but the increase is not much larger than the estimated variance in the data. Also, there is practically no difference in the observed passage period for laminar or turbulent initial conditions – at least at $\lambda = 0.65$. (The dependence of vortex spacing upon speed ratio is not predicted by application of a Galilean transformation, since all lengthscales must be proportional to $\Delta U t$ in accordance with (2). Therefore a ratio of lengthscales such as $T_p \overline{U}/\delta_\omega$ would be predicted to be a constant.) The least-squares straight line shown in figure 6 is

$$\frac{T_p \overline{U}}{\delta_\omega} = 0.54\lambda + 4.0. \tag{6}$$

3.3. *Spanwise correlation of vortex structure*

In a previous paper (Browand & Troutt 1980) we discussed the spanwise extent of the vortex structure at the single speed ratio $\lambda = 0.81$. The technique was to cross-correlate longitudinal velocity fluctuations at two spanwise locations z and $z + \Delta z$ for various downstream positions. Figure 7 gives the maximum cross-correlation in coefficient form for pairs of velocities separated by Δz (using a rake of 12 hot wires), but now for the speed ratio $\lambda = 0.56$. (The maximum cross-correlations were computed digitally by fitting a parabola through the point at zero time delay and two points at small positive and negative time delays.) The correlation coefficient,

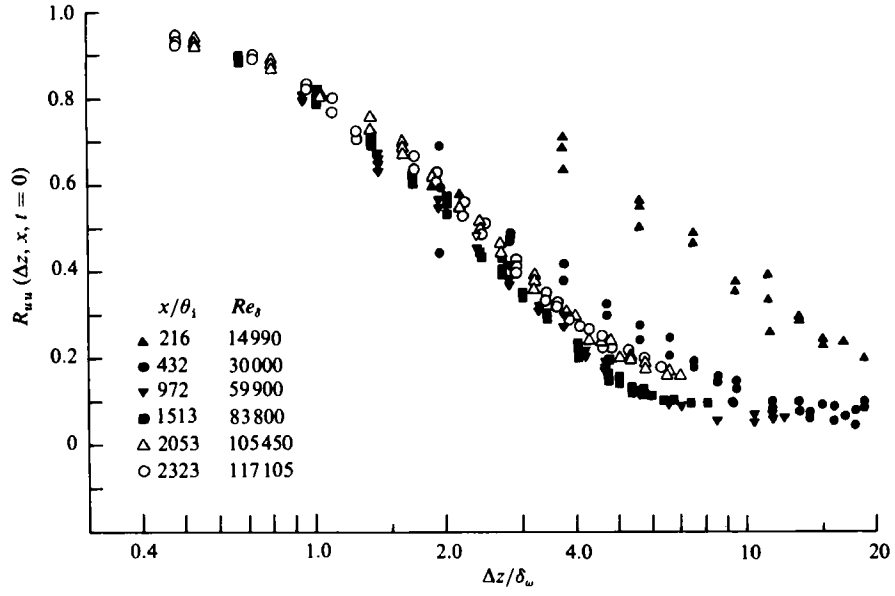

FIGURE 7. Spanwise correlation of longitudinal velocity fluctuation along the ray $y/\theta = 6$ for many downstream positions. The speed ratio is $\lambda = 0.56$. Data from many spanwise locations are shown.

plotted against spanwise separation normalized by the local layer thickness, exhibits the same behaviour as the previous result at higher speed ratio. Namely, the correlation between two points of fixed separation is initially very high. As downstream distance increases, this correlation drops rapidly, then begins to rise again – this time linearly with increase in x. Remember that δ_ω also increases linearly with x in this downstream region. When the results are displayed (figure 7) as a function of $\Delta z/\delta_\omega$ rather than Δz the correlation distribution approaches an asymptotic shape and remains unchanged with further increases in distance.

A similar result is obtained at all speed ratios investigated. Rather than plot these individually, figure 8 presents only the asymptotic distribution for each speed ratio. The result for the turbulent initial boundary layer is also shown. The correlation distributions are close but not quite identical. There is a residual dependence upon λ – what might be termed fine structure. In figure 9 the spanwise separation $\Delta z/\delta_\omega$ corresponding to 40% correlation displays a linear dependence upon λ. Values for $\lambda x/\theta_i > 600$ have been averaged for each speed ratio to produce the error bars shown. Combining these results with the autocorrelations presented earlier (figure 6) shows the large vortex structures to be – on the average – farther apart in the streamwise direction and less correlated across the span as the speed ratio increases. The asymptotic result for the turbulent initial boundary layer lies above the laminar data, by an amount larger than the estimated error. The reason is that, although the correlation at fixed separation is about 10% greater for the laminar boundary-layer case, the local thickness of the mixing layer is considerably smaller (about 25% less) for turbulent initial conditions. Here again, the two initial conditions produce small, but demonstrably lasting, differences in flow structure.

A transition point x_T can be defined using the approach of the spanwise correlations toward their far-downstream values. First, the differences between $\Delta z/\delta_\omega$ for 40% correlation and the asymptotic values in figure 9 are plotted as a function of $\lambda x/\theta_i$.

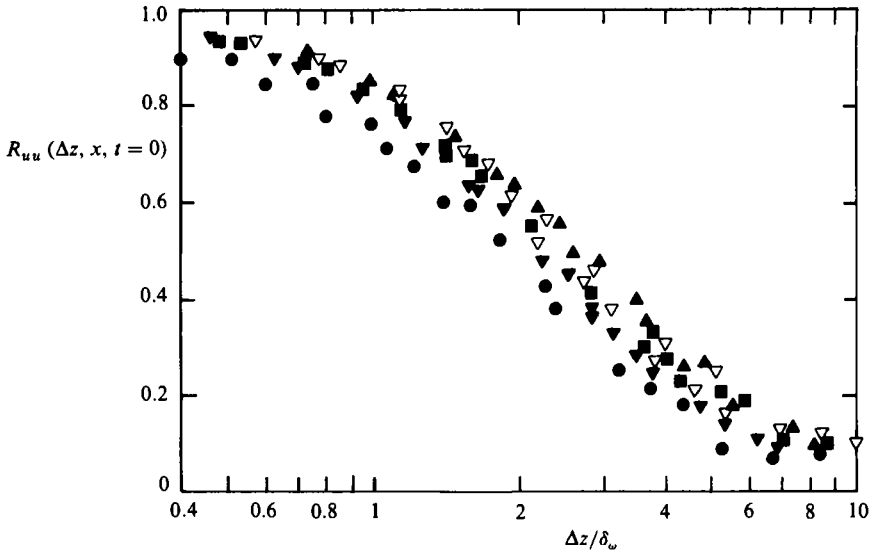

FIGURE 8. The asymptotic spanwise correlation distribution for different speed ratios: ●, $\lambda = 0.81$; ▼, 0.65; ▽, 0.65 (turbulent boundary layer); ■, 0.56; ▲, 0.41.

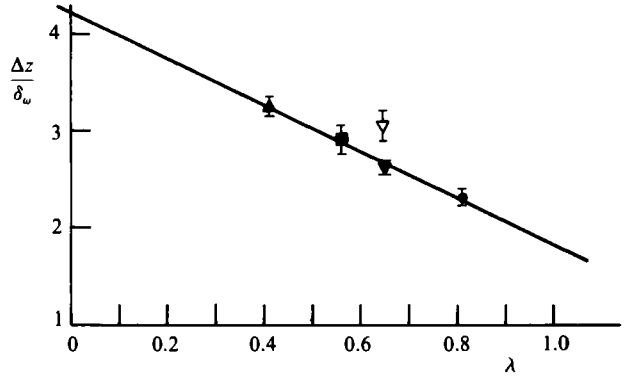

FIGURE 9. The asymptotic spanwise separation for 40% correlation as a function of speed ratio. Bars indicate estimated variance.

All data for $\lambda x/\theta_i < 300$ for the various speed ratios are used in figure 10. A reasonable fit is obtained with the form

$$\frac{\Delta z}{\delta_\omega} - \left(\frac{\Delta z}{\delta_\omega}\right)_\infty = \left[\left(\frac{\Delta z}{\delta_\omega}\right)_i - \left(\frac{\Delta z}{\delta_\omega}\right)_\infty\right] \exp\left(-\frac{\lambda x}{\theta_i}\frac{1}{\tau}\right), \tag{7}$$

where the subscripts i and ∞ refer respectively to the initial and final values. Excluding the two extreme points, and the points corresponding to turbulent initial conditions, a least-squares linear fit gives

$$\left(\frac{\Delta z}{\delta_\omega}\right)_i - \left(\frac{\Delta z}{\delta_\omega}\right)_\infty = 35.4, \tag{8}$$

$$\tau = 65.5. \tag{9}$$

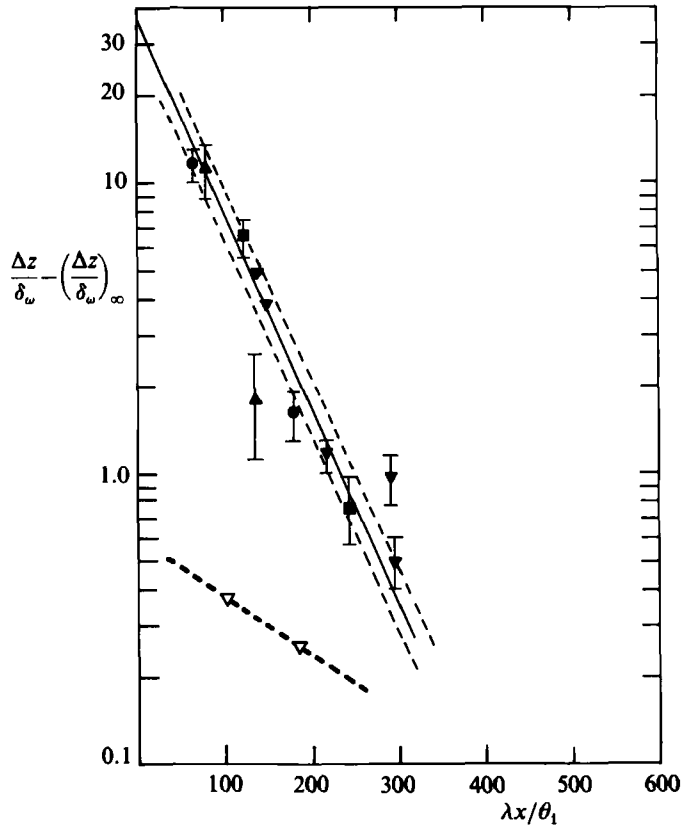

FIGURE 10. The approach of the spanwise separation for 40% correlation toward the asymptotic (limiting) value. ●, $\lambda = 0.81$; ▼, 0.65; ▽, 0.65 (turbulent boundary layer); ■, 0.56; ▲, 0.41.

The transition distance is defined to be the point where the spanwise correlation falls to within 20% of the asymptotic value. Since the asymptotic correlation values depend upon speed ratio, the values of transition distance determined from figure 10 will also be slightly different:

$$\left.\begin{aligned} \frac{\lambda x_T}{\theta_i} &= 260\text{–}282, \\ \lambda &\to 0.41\text{–}0.81. \end{aligned}\right\} \tag{10}$$

The data are probably not accurate enough to give confidence in this weak trend. An estimate of the accuracy of the least-squares line suggests the simpler result

$$\frac{\lambda x_T}{\theta_i} = 270 \pm 15 \tag{11}$$

independent of speed ratio.

The sensitivity of the transition criterion to Reynolds-number variation can also be obtained. Figure 11 demonstrates the range of experimental Reynolds number in two ways, using as the lengthscale either the initial integral thickness or the local mixing-layer thickness at transition. The lined block shows the range of the transition-distance estimate – without regard to speed ratio – while the circles correspond to the result expressed in (10). A change of 65% in $\Delta U \theta_i/\nu$ corresponds

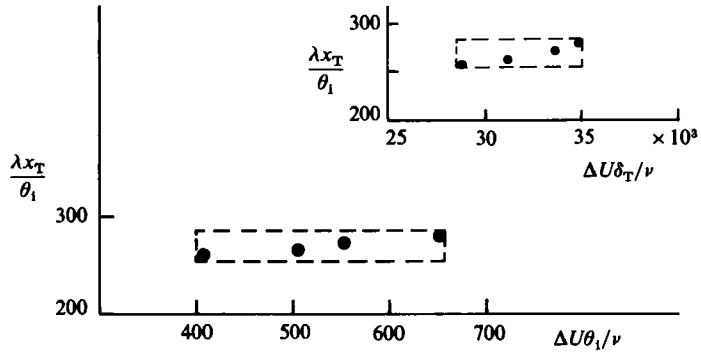

FIGURE 11. The distance x_T required to achieve the asymptotic (limiting) spanwise correlation distribution as a function of Reynolds number.

– at most – to an 8 % change in transition distance. Alternatively, a 25 % change in local Reynolds number could (possibly) be associated with the same change. The Reynolds number does not seem to be an important parameter in the establishment of asymptotic vortex structure. However, a wider range of values would have to be investigated for a more definite conclusion.

When the mixing layer originates from a turbulent boundary layer the achievement of asymptotic correlation follows a different path. The region of very high spanwise correlation near the origin is missing (figure 10). The correlation is still about 20 % larger in this initial region, and decreases slightly as downstream distance increases.

3.4. *Velocity-field visualizations*

The cross-correlation measurements are useful in describing the approach to asymptotic structure, but they give little information about the instantaneous flow structure responsible for establishing this correlation. A better physical picture is obtained by displaying a sequence of instantaneous outputs from the 12 hot wires spaced across the span. Several such visualizations are shown isometrically in figure 12. The vertical coordinate is the normalized velocity fluctuation as a function of spanwise position Δz and an equivalent downstream lengthscale $t\overline{U}$. The sign of the signals has been reversed, so that a positive fluctuation peak corresponds to a vortex immediately beneath. The structure is best revealed by the dark bands, which are the backsides of the undulations representing the passage of vortex cores. The most important conclusion is that virtually all the vortices can be traced continuously across the span of the wind tunnel – they are very long. Vortices are, however, often skewed or they may contain branching connections with neighbouring vortices. These irregularities reduce the spanwise correlation. The estimate of spanwise length obtained from an isocorrelation contour is a measure of the average distance between spanwise irregularities – not a measure of the length of the vortices themselves. Globally, the structure appears strongly oriented across the span. There can be no confusion in figure 12, for example, between the spanwise and the streamwise coordinate directions. Browand & Troutt (1980) termed this structure quasi-two-dimensional.

The first three isometrics in figure 12 show the velocity field at three downstream stations for $\lambda = 0.65$: (*a*) near the origin, where the organization is extremely high; (*b*) near the position where the spanwise correlation has fallen to its lowest value; and (*c*) farther downstream, well into the asymptotic regime. The isometrics (*b*) and

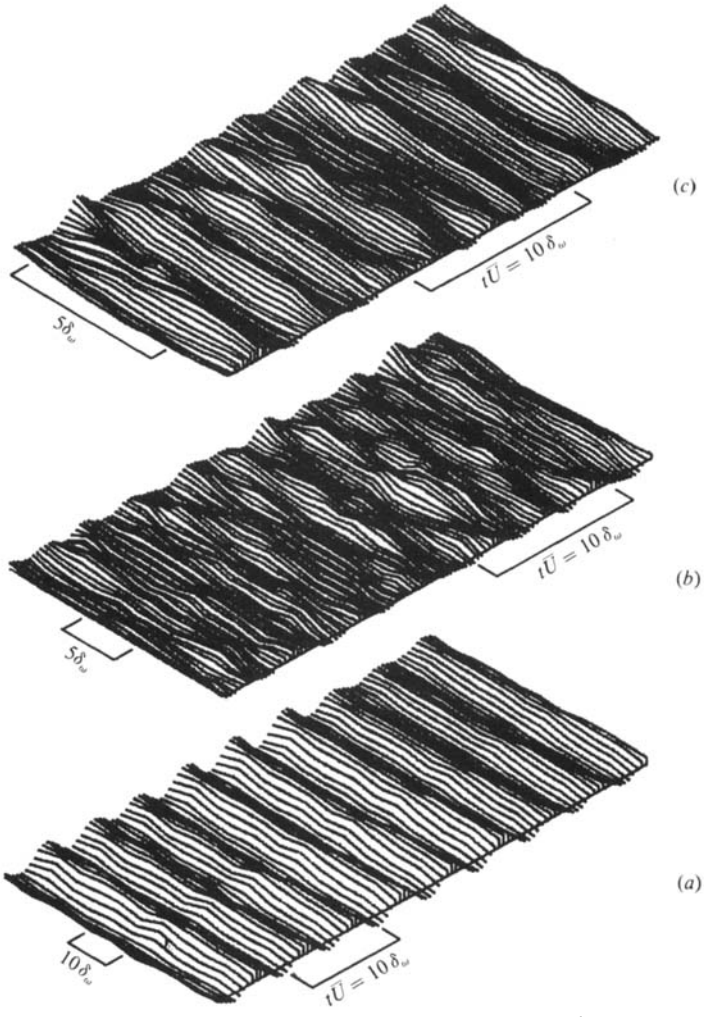

FIGURE 12 (*a*)–(*c*). For caption see opposite.

(*c*) have the same spanwise extent, 66 cm, and clearly show different degrees of correlation. The downstream position of (*b*) is 20.3 cm; that of (*c*) is 71.1 cm. A spanwise length equal to five local vorticity thicknesses, and a time $t\bar{U} = 10\delta_\omega$, are shown as appropriate dimensional scales. Isometric (*a*) is 2.5 cm from the origin. The correlation is extremely high. To improve spanwise resolution where the mixing layer is thin, the array was shortened to 12.7 cm. A spanwise length equal to $10\delta_\omega$ and an equivalent time $t\bar{U} = 10\delta_\omega$ are shown for scale. Figures 12 (*d*) and (*e*) compare asymptotic structure for the speed ratios $\lambda = 0.41$ and 0.56, respectively. The remaining isometric (*f*) corresponds to the condition of a turbulent initial boundary layer for $\lambda = 0.65$.

3.5. *Ends counting: a measure of the irregularity of vortices*

An equivalent visualization can be obtained by passing an imaginary plane through the previous isometric at a fixed fluctuation threshold. Figure 13 shows a topographical map in which the darkened areas represent fluctuation above the long-time mean. Thus darkened areas can be associated with vortex structure, and white areas with

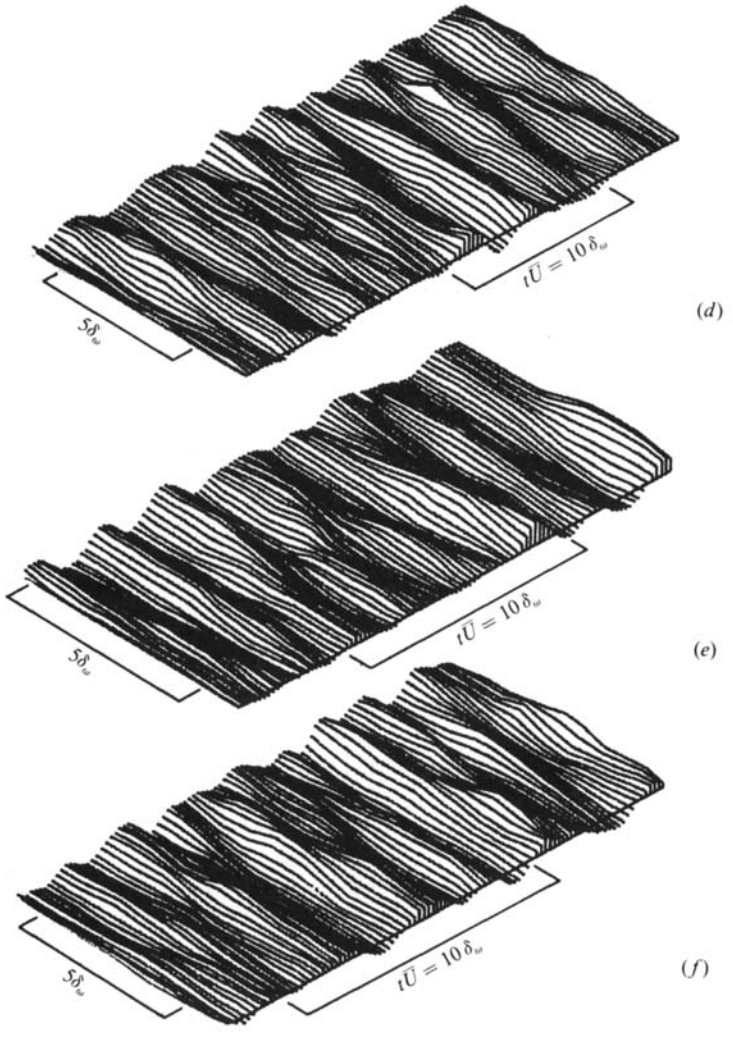

FIGURE 12. Space–time visualizations of the longitudinal-velocity fluctuation field recorded with a spanwise hot-wire rake placed at $y/\theta = 6$: (*a*) $x/\theta_1 = 56$, $\lambda = 0.65$; (*b*) $x/\theta_1 = 452$, $\lambda = 0.65$; (*c*) $x/\theta_1 = 1580$, $\lambda = 0.65$; (*d*) $x/\theta_1 = 2100$, $\lambda = 0.41$; (*e*) $x/\theta_1 = 2324$, $\lambda = 0.56$; (*f*) turbulent boundary layer, $x/\theta_1 = 1192$, $\lambda = 0.65$. Lateral extent of rake = 12.7 cm for (*a*) and 66 cm for (*b*)–(*f*).

the space between vortices (spanwise distance is horizontal, time is vertical). The four cases correspond to the appropriate isometric visualizations in figure 12. The topology is even more evident here. Vortices extend across the span, but often with much skewness and branching (cf. vortex *A* in (*d*)). Occasionally a vortex disappears, as at *B* or *C*. These serious dislocations in the vortex structure are referred to as ends. There are several possible explanations for their presence. Although a vortex cannot simply end in the flow, the vorticity within the tube could become so diffuse that the vortex is unrecognizable. We could legitimately call this an end. Alternatively, the vortex may be continuous, but dip down locally, away from the plane of the probes – producing an apparent end. We cannot distinguish between these two circumstances, so our end-counting statistics will overestimate the number of true ends. However,

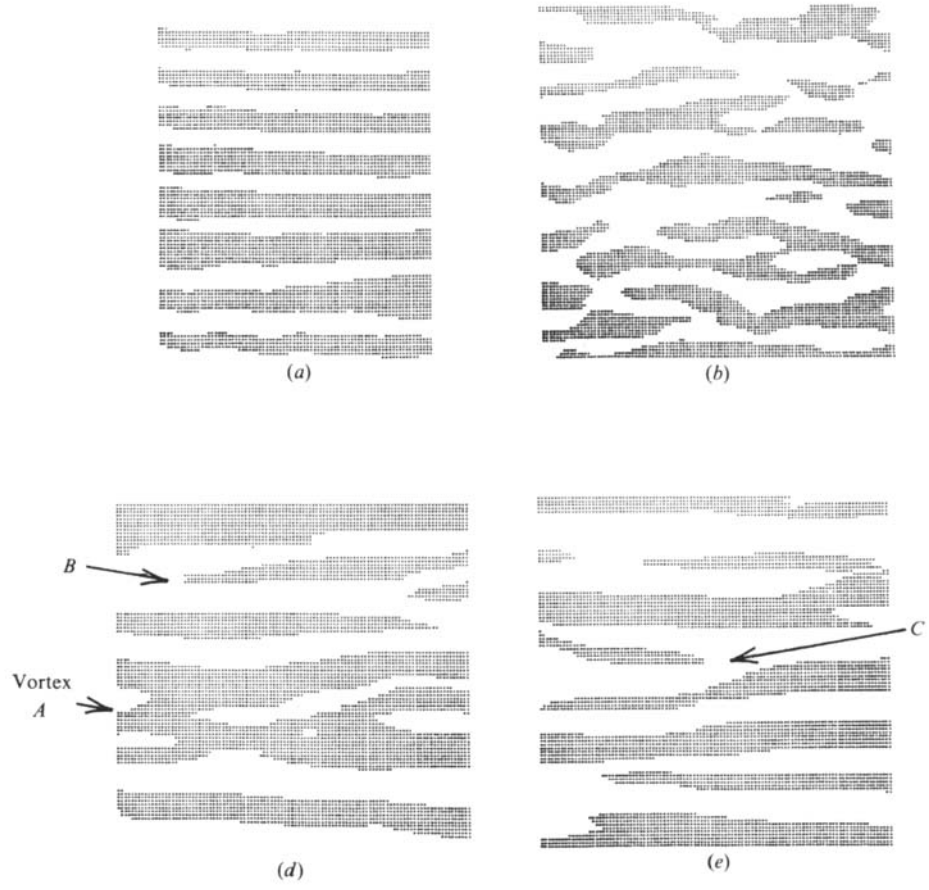

FIGURE 13. Topological plots of the longitudinal-velocity fluctuation field. Darkened regions correspond to passage of vortex cores (i.e. to times and positions where velocity fluctuation is negative). (*a*), (*b*), (*d*) and (*e*) correspond to the respective parts of figure 12. Horizontal axis is spanwise position, vertical axis is time. Examples of vortex terminations, or ends, are observed at *B* and *C*.

either situation may be regarded as a significant alteration in the regularity of the vortex structure.

An algorithm was written to locate and count ends. Quite simply, any spanwise feature that touches both side boundaries of the array has no interior end by our definition. Thus there are no ends in figure 13(*a*), and three each in (*d*) and (*e*). The method of locating ends was based upon comparing spanwise segments above the threshold (zero threshold in this case) at two adjoining instants in time. Overlapping segments, or continuations, are accounted for, as are new segments or terminated segments. The program made mistakes approximately 3% of the time, but it failed to find an end about as often as it added an extra end. Figure 14 shows the distribution of ends across the span at four downstream stations for speed ratio $\lambda = 0.65$. Record lengths corresponding to 1500–3500 passage periods were searched. The span was divided into 10 bins of equal size. The solid line is the spanwise mean value, and the dotted lines are $\pm 2\sigma$ from the mean. It is concluded that the probability of finding an end is independent of spanwise position, with the exception of the near-wall regions at the two farthest downstream locations.

The number of ends counted is now used to make an additional, independent

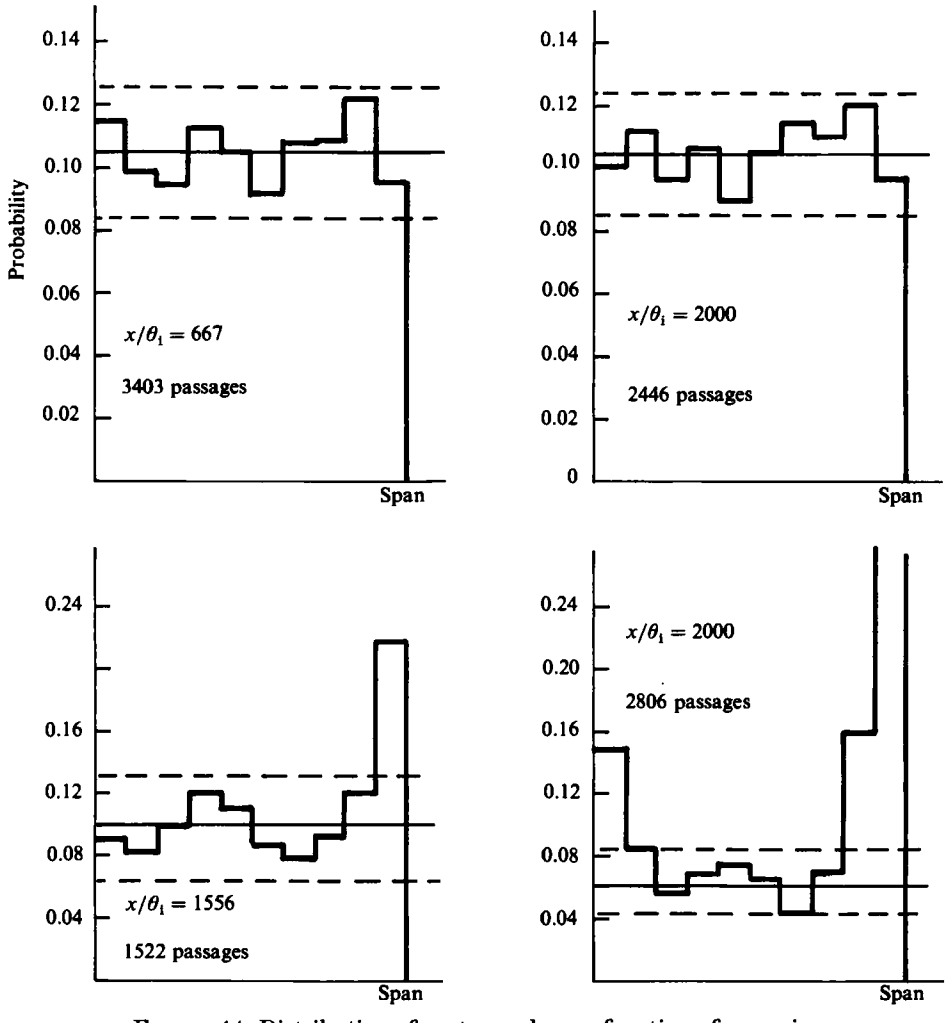

FIGURE 14. Distribution of vortex ends as a function of spanwise position for several downstream stations.

estimate of the degree of organization (or lack of organization) in the mixing layer. For, if the flow becomes more disorganized with increasing downstream distance, one would expect an increase in the number of ends appearing in a given span over an appropriate time interval. We take a unit of span equal to the local mixing-layer thickness and a unit of time $T = \delta_\omega/\overline{U}$. The number of ends occurring in this area is plotted in figure 15 for various speed ratios and various downstream positions. *The number of ends in the space–time area* $\delta_\omega(\delta_\omega/\overline{U})$ *does not increase, but becomes independent of downstream position.* This again establishes a limit for the degree of disorganization of the large vortices. The number of ends (~ 0.025 in area $\delta_\omega \delta_\omega/\overline{U}$) is sensitive to the threshold used. For higher thresholds, corresponding to a lower ratio of dark-to-light area in figure 13, more ends would be counted. At lower thresholds the opposite would be true. This sensitivity seems unavoidable, and we have chosen the threshold that makes the most physical sense – the boundary between positive and negative signal with respect to a time-averaged mean. (This corresponds to equal light and dark area in figure 13.) The conclusion regarding uniformity in the

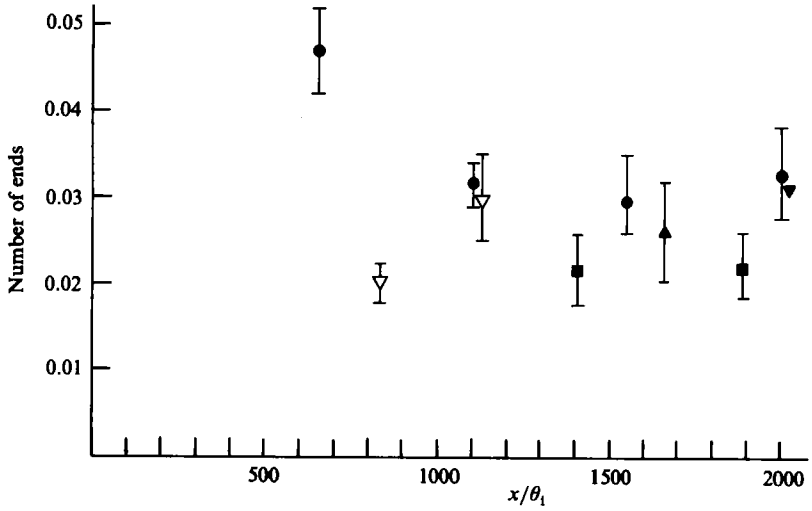

FIGURE 15. The number of vortex ends recorded in a space–time area $\delta_\omega(\delta_\omega/\overline{U})$ as a function of downstream distance. ●, $\lambda = 0.81$; ▼, 0.65; ▽, 0.65 (turbulent boundary layer); ■, 0.56; ▲, 0.41.

distribution of ends across the span, and the conclusion that the number of ends counted becomes independent of downstream distance, are *not* significantly affected by the threshold.

The number of ends, once obtained, can be used to estimate an average spanwise length for the vortices. (This estimate was suggested to the authors by Anatol Roshko during an early presentation of these results.) Combining data for all speed ratios, the average number of ends is about 0.025. Therefore there are

$$1 \text{ end in area } 40\delta_\omega(\delta_\omega/\overline{U})$$

or

$$2 \text{ ends in area } 80\delta_\omega(\delta_\omega/\overline{U}).$$

From figure 6, the average time spacing of vortices is $4.3\delta_\omega/\overline{U}$. The average spanwise length is obtained as the estimate

$$\text{length} = \frac{80\delta_\omega(\delta_\omega/\overline{U})}{4.3\delta_\omega/\overline{U}} \approx 18\delta_\omega. \tag{12}$$

This is a much better measure of the length of individual vortex structures, since it does not penalize irregularities along the span. Referring again to the first paragraph of this subsection, we note that this value must still underestimate the true length of vortex structures.

4. Concluding remarks

4.1. *The transition criterion*

The measurements of spreading rate, vortex spacing and spanwise cross-correlation all suggest that the large vortices in the mixing layer undergo a reorganization after initial laminar formation, and rapidly develop a characteristic structure that is independent of further increase in downstream distance. The distance to establish this asymptotic state – the transition distance – is characterized by

$$\frac{\lambda x_T}{\theta_i} \approx \text{constant}, \tag{13}$$

independently of Reynolds number as far as our observations can judge. This transition criterion has a simple physical interpretation. It implies that asymptotic structure is established after a fixed number of pairings or doublings of mixing-layer thickness. The thickness δ_T at transition is related to the initial mixing-layer thickness by

$$\delta_T = 2^n \delta_i, \tag{14}$$

where n is the number of doublings (pairings). There is some arbitrariness in the choice of the constant in (13), but if the spanwise correlation measurements are used the value is about 270. Appealing to figure 4(*c*) indicates that the mixing layer at transition is about 12 times the initial thickness – giving a value for n between 3 and 4.

The mixing layer develops a large-scale vortex structure even when the boundary-layer flow is made turbulent. In the past, laminar and turbulent initial conditions have often been viewed as separate circumstances. Here we emphasize the similarities that many of our results clearly demonstrate. Of course there are differences in the way the vortex structure develops initially. Our limited experiments with turbulent initial conditions do not allow generalizations for all speed ratios, but it is worthwhile summarizing the various results observed at $\lambda = 0.65$. Vortex structure must arise from an instability similar to the laminar instability. We might imagine a competition between the instability mechanism, whereby vorticity is collected and organized, and the diffusive spread of vorticity due to residual boundary-layer turbulence. Figure 5 shows – in spite of the enhanced diffusion – that vortex structure appears at an early stage and at a non-dimensional frequency of the same order as the initial laminar-instability frequency. However, the lower mean growth rate for turbulent conditions (figure 4*c*) suggests that this vortex structure is initially weaker than the laminar flow structure. These initial vortices are also considerably less correlated across the span, as shown in figure 10. Again this is evidence of weaker structure than is initially present in the laminar instability. In a sense, the mixing layer that develops from a turbulent boundary layer begins closer to its final condition – there is no strong transition.

4.2. *Permanence of structure*

The development of a large vortex structure that becomes independent of downstream distance is strong experimental support for the continued presence of these features. In fact we believe it is the most reliable quantitative evidence demonstrating the perseverance of vortices at large Reynolds numbers. If the structure were eventually to disappear, one would have to imagine transition to yet another asymptotic structure farther downstream. While this is possible, it seems unlikely, and there is presently no experimental support for such an additional transition.

There is much other experimental evidence that supports the contention that the quasi-two-dimensional vortex structure described here must be the central element in any dynamical description of the mixing layer. Browand & Weidman (1976) demonstrated that vortex pairing was associated with Reynolds-stress production in a mixing layer at Reynolds numbers of order 10^3. The lack of effective experimental techniques, in the absence of applied forcing, has hampered observations at higher Reynolds numbers, and one must rely somewhat on circumstantial evidence. Hussain & Zaman (1981) have shown that Reynolds stress favourable to the production of turbulence is associated with pairing in the mixing layer of an axisymmetric jet forced acoustically. Browand & Ho (1983) argue that interaction between large vortices (pairing) is the only effective means of generating the instantaneous momentum fluxes responsible for maintaining the energy of the turbulence. Wygnanski & Oster (1982)

have demonstrated that Reynolds stress, and therefore the state of the turbulence, can be manipulated by controlling the interactions between vortices. When pairing is inhibited, the Reynolds stress changes sign completely, and the turbulence loses energy (see also the review by Ho & Huerre 1984). Koop & Browand (1979) have observed the behaviour of the mixing layer in a stratified fluid. The vortices initially increase their scale by pairing, but at a certain point the pairing is inhibited by the stable stratification. The large vortices are obliterated, turbulent intensity decays and the flow approaches a laminar state. Apparently, the self-preserving mixing layer can only exist if vortex interactions are occurring.

The authors appreciate the financial support of both the Office of Naval Research, Fluid Dynamics and Oceanography Programs, and the National Science Foundation, Engineering Fluid Dynamics Program.

REFERENCES

Bernal, L. P. 1981 The coherent structure of turbulent mixing layers. I. Similarity of the primary vortex structure. II. Secondary streamwise vortex structure. Ph.D. thesis, California Institute of Technology.

Bernal, L. P., Breidenthal, R. E., Brown, G. L., Konrad, J. H. & Roshko, A. 1979 On the development of three-dimensional small scales in turbulent mixing layers. In *Proc. 2nd Turbulent Shear Flow Symp., Lond.*

Breidenthal, R. E. 1981 Structure in turbulent mixing layers and wakes using a chemical reaction. *J. Fluid Mech.* **109**, 1–24.

Browand, F. K. & Ho, C. M. 1983 The mixing layer: an example of quasi two-dimensional turbulence. In *Two-Dimensional Turbulence: J. Méc. Théor. Appl. Special Suppl.*, pp. 99–120.

Browand, F. K. & Latigo, B. O. 1979 Growth of the two-dimensional mixing layer from a turbulent and non-turbulent boundary layer. *Phys. Fluids* **22**, 1011–1019.

Browand, F. K. & Troutt, T. R. 1980 A note on spanwise structure in the two-dimensional mixing layer. *J. Fluid Mech.* **97**, 771–781.

Browand, F. K. & Weidman, P. D. 1976 Large scales in the developing mixing layer. *J. Fluid Mech.* **76**, 127–144.

Brown, G. L. & Roshko, A. 1971 The effect of density difference on the turbulent mixing layer. *AGARD-CP*-93, pp. 23–35.

Brown, G. L. & Roshko, A. 1974 On density effects and large structure in turbulent mixing layers. *J. Fluid Mech.* **64**, 775–816.

Ho, C. M. & Huang, L. S. 1982 Subharmonics and vortex merging in mixing layers. *J. Fluid Mech.* **119**, 443–473.

Ho, C. M. & Huerre, P. 1984 Perturbed free shear layers. *Ann. Rev. Fluid Mech.* **16**, 365–423.

Hussain, A. K. M. F. & Zaman, K. B. M. Q. 1981 The 'preferred mode' of the axisymmetric jet. *J. Fluid Mech.* **110**, 39–71.

Jimenez, J., Martinez-Val, R. & Rebollo, M. 1979 On the origin and evolution of three-dimensional effects in the mixing layer. *Univ. Politec. Madrid, Internal Rep.* DA-ERO-79-G-079.

Konrad, J. H. 1976 An experimental investigation of mixing in two-dimensional turbulent shear flows with applications to diffusion-limited chemical reactions. *Caltech. Internal Rep.* CIT-8-PU.

Koop, C. G. & Browand, F. K. 1979 Instability and turbulence in a stratified fluid with shear. *J. Fluid Mech.* **93**, 135–159.

Monkewitz, P. A. & Huerre, P. 1982 The influence of the velocity ratio on the spatial instability of mixing layers. *Phys. Fluids* **25**, 1137–1143.

Winant, C. D. & Browand, F. K. 1974 Vortex pairing, the mechanism of turbulent mixing layer growth at moderate Reynolds number. *J. Fluid Mech.* **63**, 237–255.

WOOD, D. H. & BRADSHAW, P. 1982 A turbulent mixing layer constrained by a solid surface. Part 1. Measurements before reaching the surface. *J. Fluid Mech.* **122**, 57–89.

WYGNANSKI, I. & FIEDLER, H. E. 1970 The two-dimensional mixing region. *J. Fluid Mech.* **41**, 327–361.

WYGNANSKI, I. & OSTER, D. 1982 The forced mixing layer between parallel streams. *J. Fluid Mech.* **123**, 91–130.